Available online at www.sciencedirect.com
SCIENCE DIRECT®
Mathematical Biosciences 193 (2005) 159–182
Mathematical Biosciences
www.elsevier.com/locate/mbs

When do mixotrophs specialize? Adaptive dynamics theory applied to a dynamic energy budget model

Tineke A. Troost *, Bob W. Kooi, Sebastiaan A.L.M. Kooijman

Faculty of Earth and Life Sciences, Department of Theoretical Biology, Vrije Universiteit, De Boelelaan 1087, 1081 HV Amsterdam, The Netherlands

Received 9 July 2003; received in revised form 19 April 2004; accepted 25 June 2004

Abstract

In evolutionary history, several events have occurred at which mixotrophs specialized into pure autotrophs and heterotrophs. We studied the conditions under which such events take place, using the Dynamic Energy Budget (DEB) theory for physiological rules of the organisms' metabolism and Adaptive Dynamics (AD) theory for evolutionary behavior of parameter values. We modeled a population of mixotrophs that can take up dissolved inorganic nutrients by autotrophic assimilation and detritus by heterotrophic assimilation. The organisms have a certain affinity for both pathways; mutations that occur in the affinities enable the population to evolve. One of the possible evolutionary outcomes is a branching point which provides an opportunity for the mixotrophic population to split up and specialize into separate autotrophs and heterotrophs. Evolutionary branching is not a common feature of the studied system, but is found to occur only under specific conditions. These conditions depend on intrinsic properties such as the cost function, the level of the costs and the boundaries of the trait space: only at intermediate cost levels and when an explicit advantage exists to pure strategies over mixed ones may evolutionary branching occur. Usually, such an advantage (and hence evolutionary branching) can be induced by interference between the two affinities, but this result changes due to the constraints on the affinities. Now, only some of the more complicated cost functions give rise to a branching point. In contrast to the intrinsic properties, extrinsic properties such as the total nutrient content or light intensity were found to have no effect on the evolutionary outcomes at all.

* Corresponding author. Tel.: +31 20 5987127; fax: +31 20 5987123.
E-mail address: tineke@bio.vu.nl (T.A. Troost).

0025-5564/$ - see front matter © 2005 Elsevier Inc. All rights reserved.
doi:10.1016/j.mbs.2004.06.010

Keywords: Mixotrophy; Specialization; Trade-off curve; Dynamic energy budget; Adaptive dynamics; Evolutionary branching

1. Introduction

In recent years, the omnipresence of mixotrophy and its important role in aquatic food webs have been increasingly recognized [1–3]. Mixotrophy is the nutritional strategy which combines autotrophic and heterotrophic feeding. Heterotrophy depends on outside sources of organic food materials; it includes feeding modes like pinocytosis (uptake of dissolved organic carbon) and phagocytosis (uptake of particulate organic material). In contrast, with autotrophy organic material can be manufactured from inorganic sources, which may be done by means of chemotrophy (using energy from specific inorganic molecules) or phototrophy (using energy from sunlight). Although many combinations of such heterotrophic and autotrophic types are possible, the term 'mixotrophy' is often reserved for the combination of phototrophy and phagotrophy [2]. This type of mixotrophy is often encountered in planktonic protists, which are the kind of organisms that we focus on in this study. Mixotrophy is a common phenomenon among these organisms, and they occur in a variety of freshwater and seawater habitats [4,1,5,6].

In the course of evolution, specialization of phototrophs and heterotrophs from a common mixotrophic ancestor has occurred several times. One of the earliest of such events can be found in the early development of prokaryotes. Probably, life started out with chemolithoautotrophs, as both organic matter and dioxide were rare at the time life emerged on earth [7,8]. Then, early in evolution, phototrophy arose among prokaryotes [9]. Subsequently, from the phototrophic machinery, the respiratory chain could evolve. This led to phototrophic organisms with a central glucose-based metabolism. Some of these prokaryotes improved their photosynthetic abilities; others, however, lost their ability to photosynthesize and specialized in heterotrophy.

Evolutionary branching occurred again later in evolution, in the eukaryotes. The first eukaryotes were heterotrophic and some acquired phototrophy by endosymbiosis. This had resulted in mixotrophic eukaryotes. Yet, in the course of evolution the majority of these mixotrophs specialized again in either the autotrophic or the heterotrophic direction [5].

Although evolutionary branching makes up an important part of evolutionary history, it is still not well understood why or under what conditions they take place. Also its relation with the environment is not quite clear, although in some taxa mixotrophy appears to be associated with oligotrophic environments (low nutrient supply). This is related to the fact that mixotrophs have access to two food sources, which increases their chances of survival during periods when one or both sources are limited [6]. Specialized organisms such as pure autotrophs and heterotrophs would then be thought to occur in eutrophic environments. Yet, mixotrophic protists are known to be very abundant in a range of eutrophic to oligotrophic waters [2].

Another, more 'intrinsic' factor that might regulate the occurrence of evolutionary branching could be the balance between costs and benefits involved in mixotrophy. Benefits include the better chance of survival mentioned above, but access to two food sources might also reduce the nutrient losses that are due to stoichiometry requirements, increasing the growth efficiency of the organism. In addition, mixotrophs may have the benefit of eating their competitors which will reduce inter-

specific competition for food, as was suggested by Thingstad et al. [6]. On the other hand, costs are related to building and maintaining the apparatus for both phototrophic and heterotrophic assimilation. In case of phototrophy, complex photosystems have to be build, as well as protection mechanisms against UV damage. For phagotrophy it might for instance be necessary to actively regulate the cell volume. Studies show that the apparatus involved in phototrophy can account up to 50% of the energy for cell synthesis, and comprises a corresponding fraction of the total cell biomass, although large differences exist between the various species [5]. Energy and biomass involved in the heterotrophic function seems much smaller, probably less than 10% of the total cell biomass [5].

In this paper we use a modeling approach to study the evolutionary branching of a population of mixotrophs. In order to keep our focus, we use a very simple model-system with a homogeneous environment. It is then studied how the evolutionary outcomes are related to intrinsic properties affecting the costs and benefits of assimilation and to extrinsic (environmental) properties such as the total carbon or nitrogen content.

In order to model the mixotroph system we use the Dynamic Energy Budget (DEB) theory, which is a modeling framework based on physiological mechanisms for the uptake and use of energy [10]. Then, to study under which conditions the mixotrophs will branch, we apply Adaptive Dynamics (AD) theory [11,12]. The mixotroph model differs in several aspects from the simple models used so far to develop AD theory. Inherent difficulties are solved by using an alternative method based on Levins' graphical approach and extended for AD. This graphical method takes into account both natural selection acting on differences in fitness between phenotypes and constraints on the possible set of phenotypes. A trade-off between two traits is shaped by the boundary of this set of possible phenotypes. Instead of assuming a specific trade-off curve, we derive the trade-off between autotrophy and heterotrophy on basis of mechanisms defining the costs and benefits of assimilation.

2. The model

2.1. Model description

We model the population of mixotrophs and its abiotic environment by means of the DEB-theory [10]. This theory is a modeling framework for metabolic processes with physiological rules for the uptake and use of resources. It respects the principles of energy and mass conservation, and stoichiometric constraints on the synthesis of biomass. We use a simplified version of the mixotroph model presented by Kooijman et al. [14] that has only one state variable for the mixotrophic organisms (biomass V) and three state variables for the environment: detritus D, dissolved inorganic carbon (DIC) and dissolved inorganic nitrogen (DIN). The latter two states consist of one chemical element only; biomass and detritus are thought of as generalized compounds containing both carbon and nitrogen and other elements, which have a fixed chemical composition. It is assumed that elements other than carbon and nitrogen are not limiting the growth of the organisms, and that the environment is assumed to be homogeneous; self-shading is neglected. The system is closed for mass, but open for energy.

The four state variables partake in five transformations: assimilation A (autotrophic or heterotrophic, A_A or A_H), growth G, maintenance M and death H; a diagram of these transformations

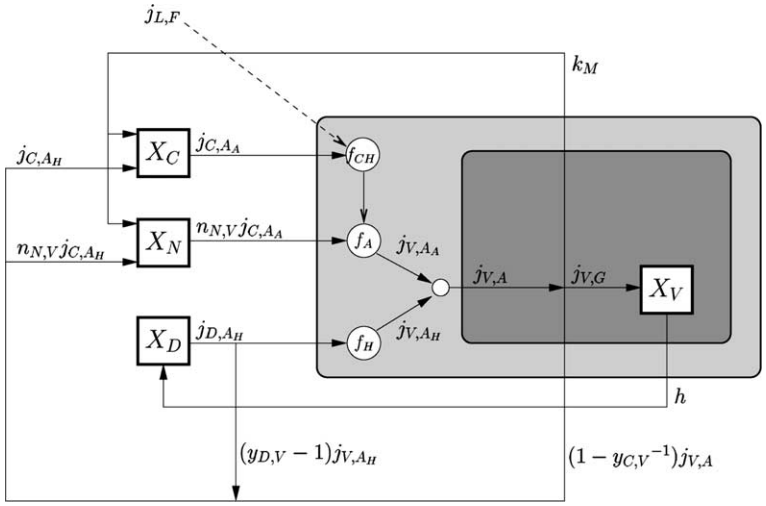

Fig. 1. Diagram of the metabolism of a mixotroph. The shaded box encloses the organism, the lighter part of which denotes its membranes containing the assimilatory machinery. A circle denotes a Synthesizing Unit (only SUs with two or more substrates are shown). The organism has one state variable for biomass X_V; the environment consists of three states: dissolved inorganic carbon X_C, dissolved inorganic nitrogen X_N and detritus X_D. Arrows indicate the structure-specific transformation fluxes.

and the corresponding fluxes is shown in Fig. 1. A mixotrophic organism assimilates the dissolved inorganic carbon and nitrogen from the environment and turns it into biomass and energy via the autotrophic pathway. When the organism dies, its biomass becomes available in the form of dead biomass (detritus) for its conspecifics via their heterotrophic pathway. Maintenance costs, overhead costs for growth and stoichiometric constraints take care of the conversion of organic carbon and nitrogen back into their inorganic form. The changes in state variables can be summarized as

$$\frac{\mathrm{d}}{\mathrm{d}t}X_\mathrm{C} = X_\mathrm{V}(j_{\mathrm{C,A}_A} + j_{\mathrm{C,A}_H} + k_\mathrm{M}) \tag{1a}$$

$$\frac{\mathrm{d}}{\mathrm{d}t}X_\mathrm{N} = X_\mathrm{V}(j_{\mathrm{C,A}_A} + j_{\mathrm{C,A}_H} + k_\mathrm{M})n_{\mathrm{N,V}} \tag{1b}$$

$$\frac{\mathrm{d}}{\mathrm{d}t}X_\mathrm{D} = X_\mathrm{V}(j_{\mathrm{D,A}_H} + h) \tag{1c}$$

$$\frac{\mathrm{d}}{\mathrm{d}t}X_\mathrm{V} = X_\mathrm{V}(j_{\mathrm{V,G}} - h) \tag{1d}$$

where X_i is the concentration of state variable i and $j_{i,j}$ is the specific flux of compound i partaking in transformation j; Both the specific maintenance rate k_M and death rate h are assumed to be constant; $n_{\mathrm{N,V}}$ is a chemical coefficient which stands for the amount of nitrogen per carbon atom in biomass. The notation used in these and following equations is introduced in Tables 1 and 2; default values of the parameters are given in Table 3.

DIC, biomass and detritus are all expressed in the amount of carbon. Therefore, the uptake flux of DIC via the autotrophic pathway $j_{\mathrm{C,A}_A}$ is equivalent to (minus) the autotrophic assimilation

Table 1
Table of symbols used for transformations and compounds

Index	Transformation	Index	Compound
A	Assimilation	C	DIC
A_A	Autotr. assim.	N	DIN
A_H	heterotr. assim.	V	Biomass
M	Maintenance	D	Detritus
H	Death		
G	Growth		

Table 2
Table of frequently used symbols for variables. Index m refers to the maximum value. In the dimension column, l means length, t time

Symbol	Dim	Interpretation
t	t	Time
X_i	$\mathrm{mol}\,l^{-3}$	Concentration of compound i
K_i	$\mathrm{mol}\,l^{-3}$	Saturation constant for compound i
$y_{i,j}$	$\frac{\mathrm{mol}\ i}{\mathrm{mol}\ j}$	Mol compound i required per mol compound j
$J_{i,j}$	$\mathrm{mol}\ i\ t^{-1}$	Flux of compound i associated with transformation j
$j_{i,j}$	$\frac{\mathrm{mol}\ i}{\mathrm{mol}\ V} t^{-1}$	Structure-specific flux of compound i
$j_{i,Am}$	$\frac{\mathrm{mol}\ i}{\mathrm{mol}\ V} t^{-1}$	Struct-spec. max assimilation flux of compound i
$j_{i,AK}$	$\frac{\mathrm{mol}\ i}{\mathrm{mol}\ V} t^{-1}$	Struct-spec. max saturation flux of compound i
$n_{i,j}$	$-$	Chemical coefficient for element i in compound j
h	t^{-1}	Hazard rate
k_{M}	t^{-1}	Maintenance rate
ρ_i	$-$	Affinity for assimilatory route i (A = autotrophic, H = heterotrophic route)
z_i	$-$	Flux ratio $j_{i,Am}/j_{i,AK}$ for compound i
z	$-$	Determines the curvature of the cost function
f_i	$-$	Scaled functional response for element/process i
r	t^{-1}	Struct-spec. growth rate
s	t^{-1}	Invasion fitness
s_i	t^{-1}	Potential fitness contributed by assimilation via route i (A or H)

flux $j_{\mathrm{V,A}_A}$, corrected with the yield coefficient $y_{\mathrm{C,V}}$. This yield coefficient accounts for the overhead costs at the transformation of carbon C into biomass V. The uptake flux of DIC via the heterotrophic pathway $j_{\mathrm{C,A}_H}$ is calculated from minus the uptake flux of detritus $j_{\mathrm{D,A}_H}$ and minus the heterotrophic assimilation flux $j_{\mathrm{V,A}_H}$, which was also corrected by $y_{\mathrm{C,V}}$. The uptake flux of detritus is equivalent to minus the heterotrophic assimilation flux $j_{\mathrm{V,A}_H}$ times the yield coefficient $y_{\mathrm{D,V}}$ for the transformation of biomass V out of detritus D. The gross growth flux $j_{\mathrm{V,G}}$ consists of the total assimilation flux $j_{\mathrm{V,A}}$ decreased by maintenance and overhead costs.

$$j_{\mathrm{C,A}_A} = -\frac{j_{\mathrm{V,A}_A}}{y_{\mathrm{C,V}}} \tag{2}$$

Table 3
Table of default values

Environmental parameters					
X_{C+}	800 μM				
X_{N+}	150 μM				
$j_{L,F}$	−5 mol/mold				
Evolutionary parameters					
ρ_A	0–1 (–)				
ρ_H	0–1 (–)				
Cost levels and function					
y^0	1.1 mol/mol				
y^A	2.5 mol/mol				
y^H	2.5 mol/mol				
y^{AH}	0.0 mol/mol				
z	1 (–)				
K_C	500 μM	z_C	10 (–)	$y_{D,V}$	1.3 mol/mol
K_N	0.1 μM	z_N	10 (–)	$n_{N,V}$	0.15 (–)
K_D	2500 μM	z_{C_H}	10 (–)	k_M	0.1 d^{-1}
$j_{V,A_A m}$	2.6 mol/mold	$j_{L,FK}$	25 mol/mold	h	0.1 d^{-1}
$j_{V,A_H m}$	2.6 mol/mold				

$$j_{C,A_H} = -j_{D,A_H} - \frac{j_{V,A_H}}{y_{C,V}} \tag{3}$$

$$j_{D,A_H} = -y_{D,V} j_{V,A_H} \tag{4}$$

$$j_{V,G} = \frac{j_{V,A}}{y_{C,V}} - k_M \tag{5}$$

The deviation in these equations from [14] is caused by the extra overhead costs that were included for building biomass. A discussion of these costs and the assimilation fluxes j_{V,A_A}, j_{V,A_H} and $j_{V,A}$ is given below.

2.1.1. Assimilation

Mixotrophs have the ability to produce biomass via two separate pathways, the autotrophic and heterotrophic pathway. In the model, a central role is played by the affinities that the organisms have for each of these two assimilatory pathways; ρ_A for the autotrophic route and ρ_H for the heterotrophic route. These affinities represent binding probabilities and therefore their values range from 0 to 1. A higher affinity may be interpreted as an increase or an improvement in the assimilation machinery that results in a higher binding probability, which in turn will lead to a higher assimilation flux.

Autotrophic and heterotrophic assimilation fluxes j_{V,A_A} and j_{V,A_H} are proportional to the affinities, the corresponding maximum assimilation rates $j_{V,A_A m}$ and $j_{V,A_H m}$, and the functional responses f_A and f_H:

$$j_{\mathrm{V,A}_A} = \rho_A j_{\mathrm{V,A}_A m} f_A \tag{6}$$

$$j_{\mathrm{V,A}_H} = \rho_H j_{\mathrm{V,A}_H m} f_H \tag{7}$$

In [14] these affinities were not included in the assimilation fluxes, but in the gross growth flux $j_{\mathrm{V,A}}$. Another difference is that here we assume that no limitation exists to the total assimilation flux $j_{\mathrm{V,A}}$ ($k \to \infty$). This flux then simply becomes:

$$j_{\mathrm{V,A}} = j_{\mathrm{V,A}_A} + j_{\mathrm{V,A}_H} \tag{8}$$

The functional responses are modeled with use of Synthesizing Units (SUs) Kooijman [10,15], which provide a simple and realistic method for calculating production fluxes at simultaneous nutrient and light limitations. Planktonic protists have a photosynthetic system that consists of two photosystems, with which they stepwise convert carbon dioxide, nitrogen and light into biomass. First, carbon dioxide and photons are bound by carriers. Then, the carbon dioxide is reduced into a carbohydrate. Nitrogen is bound and, together with the carbohydrates, synthesized into biomass. This process can be modeled by coupling several SUs. Binding fluxes of carbon f_{C} and nitrogen f_{N} can be calculated by a simple one-substrate SU; the reduction rate of carbon f_{CH} can be calculated by a complementary SU for which both carbon and electrons are essential. Finally, f_A can be calculated with again a complementary SU. These processes can be represented by the following equations:

$$\begin{aligned}
f_{\mathrm{C}} &= \frac{X_{\mathrm{C}}}{K_{\mathrm{C}} + X_{\mathrm{C}}} \\
f_{\mathrm{CH}} &= \frac{1 + z_{\mathrm{C}}^{-1}}{1 + a^{-1} + b^{-1} - (a+b)^{-1}}; \quad a = z_{\mathrm{C}} f_{\mathrm{C}}; \quad b = \frac{-J_{\mathrm{L,F}}}{J_{\mathrm{L,FK}}} \\
f_{\mathrm{N}} &= \frac{X_{\mathrm{N}}}{K_{\mathrm{N}} + X_{\mathrm{N}}} \\
f_A &= \frac{1 + z_{\mathrm{N}}^{-1} + z_{\mathrm{CH}}^{-1} - (z_{\mathrm{N}} + z_{\mathrm{CH}})^{-1}}{1 + a^{-1} + b^{-1} - (a+b)^{-1}}; \quad a = z_{\mathrm{N}} f_{\mathrm{N}}; \quad b = z_{\mathrm{CH}} f_{\mathrm{CH}}
\end{aligned} \tag{9}$$

where K_i is the saturation constant for compound i and z_i a scaling parameter that weighs the contributions of carbon C, carbohydrates CH and nitrogen N. Light influx $J_{\mathrm{L,F}}$ (negative, because photons flow in) is scaled with parameter $J_{\mathrm{L,FK}}$ so that a multiplication of these two fluxes with an arbitrary number (different from zero) has no effect. The light influx can be taken proportional to the solar irradiance (photon flux per unit of surface area of water/air boundary layer). For a detailed discussion on modeling photosynthesis by means of SUs the reader is referred to Kooijman [10,14].

The functional response of the heterotrophic route f_H depends on the binding of detritus, which can be represented by a one-substrate SU:

$$f_H = \frac{X_{\mathrm{D}}}{K_{\mathrm{D}} + X_{\mathrm{D}}} \tag{10}$$

in which K_{D} is the saturation constant for detritus. In [14] a parallel processing SU was used that complemented detritus with DIN to synthesize biomass; the two models are equal when nitrogen density does not limit the heterotrophic assimilation flux ($K_{N_{\mathrm{V}}} \to 0$).

At the transformation of resources into biomass, overhead costs have to be paid; these costs are quantified by the yield coefficient $y_{C,V}$ (11). The value of this yield coefficient is related to the affinities for assimilation, as among the overhead costs are the costs that are associated with the building of assimilation machinery. Depending on the mechanisms assumed, various relations between overhead costs and affinities result. These costs consist of three parts: (1) a constant 'base' cost y^0, specifying the costs involved in biomass production apart from the assimilation machinery; (2) costs associated with the increase in or the improvement of the assimilation machinery, a relation that can be either linear ($z = 1$), convex ($z < 1$) or concave ($z > 1$); the absolute increase in these costs are specified by the parameters y^H and y^A; (3) other costs that are proportional to the product of the two affinities; their relative increase is specified by the parameter y^{AH}. Together, these three parts make up the (flexible) function for the yield coefficient $y_{C,V}$:

$$\begin{aligned} &\text{costs} = \text{base costs} + \text{costs for ass.machinery}(A_A \text{ and } A_H) + \text{extra costs} \\ &y_{C,V} = y^0 + y^A(1-(1-\rho_A)^z) + y^H(1-(1-\rho_H)^z) + y^{AH}\rho_H\rho_A \end{aligned} \tag{11}$$

2.1.2. Population and ecosystem

The DEB theory takes the organism's uptake to be proportional to its surface area and maintenance to be proportional to its (structural) mass. Because we assume here that an organism's surface area is proportional to its mass, the distinction between the individual and the population is eliminated in the expressions for the fluxes. The system is closed for mass, but open for energy and is started up containing only one (monomorphic) population of mixotrophs. Because the mixotrophs are capable of both autotrophic and heterotrophic assimilation, all essential recycling of carbon and nutrients is installed and a continuous material cycling through the ecosystem is possible. So, although only a single population is involved, we can regard the mixotrophs and their environment as a complete ecosystem.

2.1.3. Evolution and specialization

Evolution is included in the system in the form of random but small mutations, i.e. heritable changes in parameters values. The mutations occur (independently) in the values of the two affinities ρ_A and ρ_H that the mixotrophs have for the two assimilatory pathways. A time scale separation is assumed between the evolutionary time scale and the population dynamical time scale, so that mutations occur only after the system has reached a steady state. Our main goal is then to derive under which conditions for the affinities the mixotroph population specializes into a dimorphic population of autotrophs and heterotrophs.

2.2. Predicting the evolutionary outcome

Predictions of the evolutionary outcome of the system are made with use of AD theory [11,12]. The fitness s of an organism with a certain phenotype (ρ_A,ρ_H) is defined as its long-term average per capita growth rate r. An important concept in AD theory is the feedback loop between population and environment; the resident population is said to 'set' the environment, which is then denoted by E_{res}. The resident population that has reached a steady state with its environment,

does not grow or shrink so that phenotypes $(\rho_{A_{\text{res}}}, \rho_{H_{\text{res}}})$ belonging to this population by definition have an invasion fitness of zero:

$$s_{\text{res}} = r(\rho_{A_{\text{res}}}, \rho_{H_{\text{res}}}, E_{\text{res}}) = 0 \tag{12}$$

When a mutant phenotype arises, it will be rare and is therefore assumed not to affect the environment in the short term. Its invasion fitness will thus be determined by its phenotype $(\rho_{A_{\text{mut}}}, \rho_{H_{\text{mut}}})$, and by the environment which was set by the residents:

$$s_{\text{mut}} = r(\rho_{A_{\text{mut}}}, \rho_{H_{\text{res}}}, E_{\text{res}}) \tag{13}$$

Mutants of a phenotype having a positive invasion fitness may be able to invade, those having a negative invasion fitness will die out. Following the invasion, a mutant may replace the resident population and become the new resident or live on in coexistence with the original population. Together, the changed population and the environment will reach a new steady state, in which the new residents will have a growth rate of zero again. It is by a series of such invasions and replacements that the population evolves towards a 'singular strategy' at which both the fitness gradients have vanished:

$$\frac{\partial s_{\text{mut}}}{\partial \rho_{A_{\text{mut}}}} = 0 \quad \text{and} \quad \frac{\partial s_{\text{mut}}}{\partial \rho_{H_{\text{mut}}}} = 0 \tag{14}$$

A phenotype is a combination of the properties or 'traits' that characterize the organisms, and all phenotypes together form the organisms' trait space. In this trait space, fitness-contour lines connect all combinations of traits that have the same invasion fitness. Such a contour plot is often thought of as a 'fitness landscape', with peaks at phenotypes that have a high fitness and valleys at those of small fitness. As invasion fitness depends on the mutant's trait values but also on the environment which was set by the resident, this landscape is different for different resident populations. The sequence of resident replacements typical to the evolutionary process then gives rise to the concept of 'changing fitness landscapes'.

The model presented here differs from the simple 'toy' models that are often used in AD theory. Not only is the mixotroph model physiologically based, but also is it two-dimensional, meaning that the organisms have two traits that are subject to evolution instead of one. The standard graphical approach in AD that uses Pairwise Invasibility Plots (PIP's) is only appropriate for one-dimensional cases and comments on the extension of the theory for multiple traits are rare [16,11]. Therefore, we use an alternative method based on Levins' graphical approach, which was extended for AD theory by Rueffler et al. [13]. The classical approach [17] is based on fixed fitness landscapes, but the extended approach does include density dependence, which leads to the changing fitness landscapes that are conditional on the resident type. With this method it is possible to classify the evolutionary behavior as a function of the curvature of the invasion boundary and the shape of the trade-off function.

Invasion boundaries are the zero-fitness contours, consisting of all those phenotypes that are selectively neutral, i.e. which neither grow nor shrink in numbers under the conditions set by the resident population. Mutants with a strategy at one side of the invasion boundary will have a negative invasion fitness and will all die out. Mutants with a strategy at the other side of the invasion boundary will have a positive invasion fitness and will potentially be able to invade. Trade-offs exist between two (beneficial) processes or traits of which not all combinations are

feasible for the organism. Together, the feasible phenotypes constitute the feasibility set, which is a subset of the total trait space. The trade-off function is shaped by the boundary of this feasibility set. For strategies on the trade-off curve an increase in either of the two traits results in a decrease of the other.

Rueffler et al. [13] explained that under certain assumptions a series of mutations will always lead towards this trade-off curve, and once it has been reached, evolution is assumed to proceed along it. The direction of further trait substitutions depends on whether the derivative of the invasion boundaries is smaller or larger than that of the trade-off curve. Whereas the trade-off curve does not depend on the environment, the invasion boundaries do depend on the environment and so they will change every time the resident population is replaced by a new population. The process of mutations followed by the replacement of the resident population will continue until the invasion boundary becomes tangent to the trade-off curve or until the border of the feasibility set is reached. In the first case the fitness gradient vanishes and a singular strategy is reached. From the shapes of trade-off curve and invasion boundaries, it can then be determined if such a singular strategy is an attractor (convergence stable) and whether it is invadable (evolutionarily stable).

Two of the possible outcomes of evolution are continuously stable strategies (CSS's) and branching points. The former are convergence stable and evolutionarily stable strategies. In other words these are attractors that can not be invaded by any mutant; the population will remain on such a strategy. The latter are convergence stable but evolutionarily unstable strategies. When arriving at a branching point any mutant is able to invade, and disruptive selection will induce the population to split up into two populations. For the mixotrophs such branching points form opportunities to specialize into separate autotrophs and heterotrophs.

In terms of Levins' extended approach a singular strategy is an *attractor* if the slope of the invasion boundaries above this strategy is larger (more negative) than the slope of the trade-off curve at the place where the two intersect; below the singular strategy the slope of the invasion boundaries must be smaller (less negative) than that of the trade-off curve. A singular strategy is *invadable* if the second derivative of the invasion boundaries is smaller (more negative) than that of the trade-off curve. From this follows that, when the invasion boundaries are known to be linear and the singular strategy is an attractor, the trade-off curve has to be convex in order to give rise to a branching point.

2.3. Levins' graphical approach applied to the mixotroph model

To find the conditions under which evolutionary branching occurs in the mixotroph model, we must first define the mixotrophs' traits, invasion fitness and trade-off function. As was discussed above, every model organism is characterized by its two trait values ρ_A and ρ_H. The values of the affinities range between 0 and 1, so the organism's trait space is the set $\mathscr{T} = \{\rho_A, \rho_H \mid 0 \leqslant \rho_A \leqslant 1 \wedge 0 \leqslant \rho_H \leqslant 1\}$. The invasion fitness s_{mut} of a mutant strategy $(\rho_{A_{\text{mut}}}, \rho_{H_{\text{mut}}})$ in an environment that is set by the resident population E_{res} is defined as its specific growth rate. This can be rewritten from Eqs. (1d) and (5) as follows:

$$s_{\text{mut}} = \frac{1}{X_{\text{V}}}\frac{\text{d}}{\text{d}t}X_{\text{V}} = \frac{j_{\text{V,A}}(\rho_{A_{\text{mut}}}, \rho_{H_{\text{mut}}}, E_{\text{res}})}{y_{\text{C,V}}(\rho_{A_{\text{mut}}}, \rho_{H_{\text{mut}}})} - k_{\text{M}} - h \tag{15}$$

in which we now denoted explicitly the arguments of the variables. $j_{\mathrm{V,A}}$ again is the total gross assimilation flux, $y_{\mathrm{C,V}}$ the yield coefficient for biomass out of carbon, k_{M} the maintenance costs and h the death rate.

As the affinities are related to both costs and benefits, they are no direct measures for invasion fitness. An expression is needed in which the affinities are translated into a partial fitness contributed by the autotrophic route and a partial fitness contributed by the heterotrophic route. By substituting (6) and (7) via (8) in (15) the separate contributions of the two trophic pathways to total invasion fitness become explicit:

$$\begin{aligned} s_{\mathrm{mut}} &= \frac{j_{\mathrm{V,A}_A}(\rho_{A_{\mathrm{mut}}}, \rho_{H_{\mathrm{mut}}}, E_{\mathrm{res}}) + j_{\mathrm{V,A}_H}(\rho_{A_{\mathrm{mut}}}, \rho_{H_{\mathrm{mut}}}, E_{\mathrm{res}})}{y_{\mathrm{C,V}}(\rho_{A_{\mathrm{mut}}}, \rho_{H_{\mathrm{mut}}})} - k_{\mathrm{M}} - h \\ &= f_{A_{\mathrm{mut}}}(E_{\mathrm{res}}) \frac{j_{\mathrm{V,A}_A m}\rho_{A_{\mathrm{mut}}}}{y_{C,V}(\rho_{A_{\mathrm{mut}}}, \rho_{H_{\mathrm{mut}}})} + f_{H_{\mathrm{mut}}}(E_{\mathrm{res}}) \frac{j_{\mathrm{V,A}_H m}\rho_{H_{\mathrm{mut}}}}{y_{\mathrm{C,V}}(\rho_{A_{\mathrm{mut}}}, \rho_{H_{\mathrm{mut}}})} - k_{\mathrm{M}} - h \\ &= f_{A_{\mathrm{mut}}}(E_{\mathrm{res}}) s_A(\rho_{A_{\mathrm{mut}}}, \rho_{H_{\mathrm{mut}}}) + f_{H_{\mathrm{mut}}}(E_{\mathrm{res}}) s_H(\rho_{A_{\mathrm{mut}}}, \rho_{H_{\mathrm{mut}}}) - k_{\mathrm{M}} - h \end{aligned} \tag{16}$$

in the last step of which we rename the grouped terms as the potential autotrophic fitness s_A and the potential heterotrophic fitness s_H. These contributions are called 'potential' because they do not include the functional responses f_A and f_H, and thus stand for the maximally attainable fitness of each trophic route.

Now that the contributions of autotrophy and heterotrophy to the invasion fitness have been separated and can be expressed in s_A and s_H, the shape of the trade-off curve and the invasion boundaries can be found much more easily. At the invasion boundaries the invasion fitness s_{mut} is zero. (16) shows that in this case the invasion boundaries become linear in s_A and s_H. Because of this, the evolutionary stability of the singular strategies can be predicted on basis of the shape of the trade-off curve alone: if the trade-off curve is concave the singular strategy will be evolutionarily stable; if it is convex the singular strategy will be evolutionarily unstable. Note that all singular strategies are also attracting (convergence stable), because autotrophs and heterotrophs are mutually dependent; their products serve as each others substrates. This means that the shape of the trade-off curve now fully determines the qualitative evolutionary outcome of the system: if the trade-off curve is concave the population will evolve towards a CSS at which it will remain; if the trade-off curve is convex a branching point will arise and the population will split up.

The trade-off curve can be visualized indirectly by the feasibility set, because it consists of this set's boundary. The feasibility set consists of all possible combinations of s_A and s_H. It is obtained by calculating for every combination of the two affinities the potential autotrophic fitness s_A and the potential heterotrophic fitness s_H; it thus is the set $\mathscr{F} = \{s_A, s_H \mid 0 \leqslant \rho_A \leqslant 1 \wedge 0 \leqslant \rho_H \leqslant 1\}$. The feasibility set can be shown by means of a contour or surface plot of the invasion fitness s_{mut} plotted against the two potential fitnesses s_A and s_H; its boundary is the trade-off curve. A complicating factor in showing the trade-off curve is that the invasion fitnesses of the mutants lying on this curve change with every resident. This can be solved by using the 'total potential fitness' instead of the invasion fitness; the total potential fitness s_{pot} is simply the sum of the two partial potential fitnesses:

$$s_{\mathrm{pot}} = s_A(\rho_A, \rho_H) + s_H(\rho_A, \rho_H) \tag{17}$$

Putting the total potential fitness on the z-axis of the contour plot (instead of the invasion fitness) will not affect the feasibility set $\mathscr{F}$ and thus not the shape of the trade-off curve. However, the total potential fitness is independent of the resident strategy, which makes it an unambiguous measure with which to represent the trade-off curve. In terms of the total potential fitness, the trade-off curve can be described as to consist of those strategies that combine a given value of ρ_H with a value of ρ_A such that the total potential fitness s_{pot} is maximal, provided that ρ_H lies between 0 and the value at which s_{pot} is highest; vice versa, it also consists of the strategies that combine a given ρ_A with a ρ_H such that s_{pot} again is maximal and ρ_A lies between 0 and the value at which s_{pot} is highest. The trade-off curve thus is the set $\mathscr{C} = \{s_A, s_H \mid (0 \leqslant \rho_A \leqslant \rho_{A_{\text{opt}}} \wedge \rho_H \mid s_{\text{pot}} = \text{maximal}) \vee (\rho_A \mid s_{\text{pot}} = \text{maximal} \wedge 0 \leqslant \rho_H \leqslant \rho_{H_{\text{opt}}})\}$.

The relation between the traits ρ_A and ρ_H and potential fitnesses s_{pot} is illustrated in Fig. 2, in which surface and (base-)contour plots of the total potential fitness are shown. The figures on the left show the total potential fitness for every combination of ρ_A and ρ_H; on the right these strategies have been translated into potential fitnesses s_A and s_H. In the base-contour plots, the feasibility set $\mathscr{F}$ now becomes visible, as does its boundary $\mathscr{C}$, which forms the trade-off curve between autotrophy and heterotrophy. Each grid cell consists of a different combination of the two affinities and thus denotes a different strategy, and each grid cell in the surface plot on the left corre-

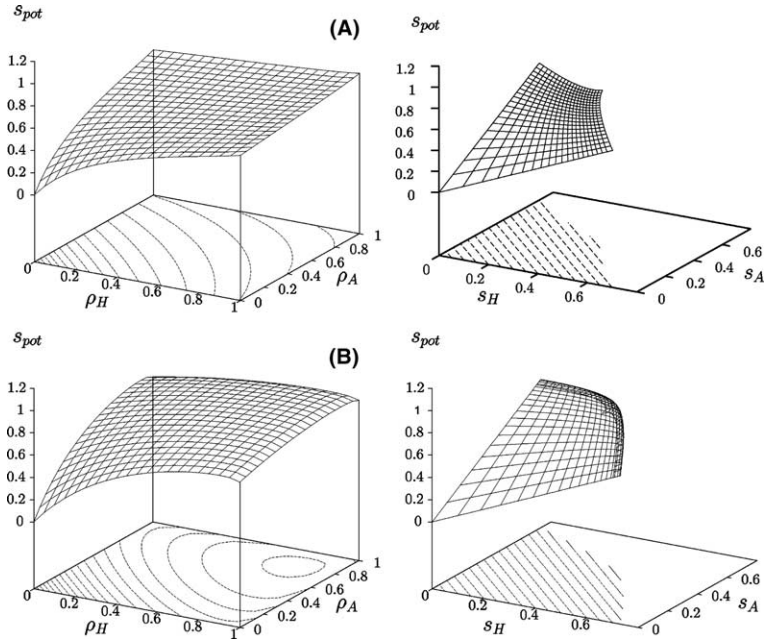

Fig. 2. Surface plots and (base-)contour plots of total potential fitness s_{pot} (17). On the left, total potential fitness is plotted for every combination of the two affinities ρ_A and ρ_H; on the right these strategies are translated into the potential autotrophic and heterotrophic fitnesses s_A and s_H. The base-contour plots in the latter figures show the feasibility sets $\mathscr{F}$, as well as their upper boundary, which are the tradeoff curves $\mathscr{C}$. (A) Optima in total potential fitness lie at the extremes of affinity trait space; the trade-off curve coincides with the boundaries of the trait space ($\mathscr{C} = \mathscr{B}$). (B) Optima in total potential fitness lie at intermediate trait values; on the right the fitness surface folds back onto itself, so that the boundaries of the trait space end up within the feasibility set.

sponds with a grid cell in the surface plot on the right. Although on the left these strategies are shown in terms of affinity values and on the right they are shown in terms of potential autotrophic and heterotrophic fitnesses, corresponding strategies have the same total potential fitness in both plots. In the first example (A) potential fitness increases monotonously in both affinities; in the second example (B) fitness optima lie at intermediate affinities.

In the plots on the right of Fig. 2 it can be seen that total potential fitness increases when approaching the trade-off curve. Another feature illustrated in these plots is the role of the constraints on the affinity trait space $\mathscr{T}$. At its boundaries, either of the affinities has a constant value of 1, while the other affinity varies. These boundaries are given by the set $\mathscr{B} = \{s_A, s_H \mid (0 \leqslant \rho_A \leqslant 1 \wedge \rho_H = 1) \vee (\rho_A = 1 \wedge 0 \leqslant \rho_H \leqslant 1)\}$. In the example (A) the trade-off curve coincides with the boundary of the trait space, $\mathscr{C} = \mathscr{B}$. In this case the shape of this trade-off curve is governed by the constraints on the affinities. In example (B) the best strategies lie at intermediate trait values, and limitations to affinity trait space do not play a role in shaping the trade-off curve.

To study the effect of various cost functions, we tested four different cost functions (11) and three levels of the costs: For the first three cost functions, costs are related to the trait values ($y^A > 0$, $y^H > 0$, $y^{AH} = 0$). For the first cost function a convex relation between affinity and costs was assumed ($z = 0.7$). This cost function implies relatively low costs for small affinities but leads to increasingly higher costs at higher affinities. For the second cost function a linear relation between affinity and costs was assumed ($z = 1$). For the third cost function a concave relation between affinity and costs was assumed ($z = 1.3$), which implies that small affinities are relatively expensive but for higher affinities costs will level off. The fourth cost function does not assume a relation between affinities and costs as such, but is proportional to the product of the affinities ($y^A = 0$, $y^H = 0$, $y^{AH} > 0$). These costs might for instance be associated with interference of intermediary products of the two pathways. Finally, three additional cost functions consisting of a combination of the fourth costs function with one of the first three ($y^A > 0$, $y^H > 0$, $y^{AH} > 0$) were tested for their effect on the shape of trade-off curve. The parameters y^A, y^H and y^{AH} were set to low (1.0), intermediate (2.5) or high values (5.0), respectively.

3. Results

Fig. 3 shows the feasibility sets $\mathscr{F}$ and trade-off curves $\mathscr{C}$ for various cost functions (rows) and at three levels of costs (columns). In the first three rows, costs are related to trait value. In the fourth row, costs are related to the combination of the two affinities. Arrows indicate the strategies where the population will end up, which in case of a CSS is at the location of the singular strategy (which may be a boundary optimum) and in case of a branching point at the two end strategies that result after branching. A solid line marks the boundaries of the affinity trait space $\mathscr{B}$. It can be seen that in many of these figures, the trade-off curve coincides with these boundaries, $\mathscr{C} = \mathscr{B}$. Although not shown, invasion boundaries are all linear, and they all intersect the feasibility set such that all singular strategies are attracting.

The figure shows that for low cost levels the feasibility sets are large, and that their size decreases and their shape flattens with increasing cost level. At low costs the singular strategy is a boundary optimum that lies in the middle of the trade-off curve; this is an attractor and it is evolutionarily stable (CSS). At high levels of costs the upper-left extreme of the trade-off curve is

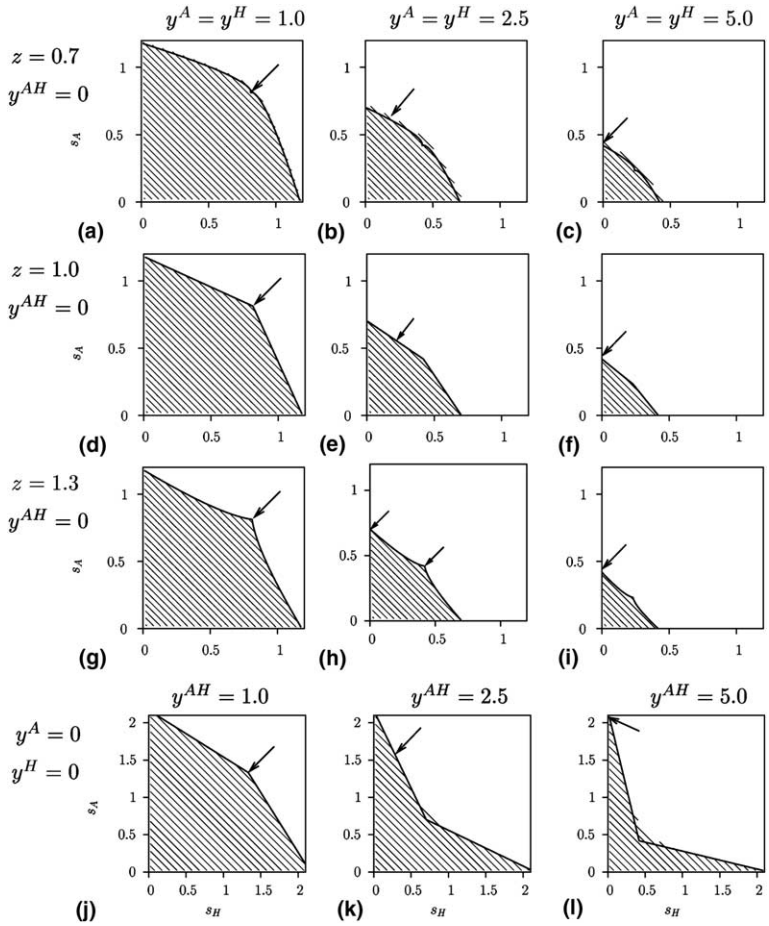

Fig. 3. Contour plots of total potential fitness s_{pot} (17) for various cost functions (rows), and for three levels of costs (columns). The contours give shape to the feasibility sets $\mathscr{F}$; their boundaries form the trade-off curves $\mathscr{C}$. Arrows indicate the evolutionary end strategies. Invasion boundaries are not shown but are all linear and intersect with the trade-off curve such that all singular strategies become attractors. The solid line other than the fitness contours shows the boundary of the affinity trait space $\mathscr{B}$, which in some cases coincides with the trade-off curve. In the first three rows, costs (11) are related to the trait values; these relations can be either convex, linear or concave. In the fourth row, costs are related to interference of intermediary products. At low costs (first column), the singular strategy is a CSS, with $\rho_H = 1$ and $\rho_A = 1$. At intermediate costs (center column), the singular strategy has shifted to the upper left of the trade-off function. Its evolutionary behavior depends on the specific cost function; At high costs (last column) the evolutionary end point has come to lie at the extreme of the trade-off curve where $\rho_H = 0$. This population is not viable and will die out.

reached. Although this strategy is attracting and evolutionarily stable, it is not viable. Intermediate levels of costs will lead to a singular strategy that lies somewhere in-between, and which in some cases again is a boundary optimum. Its evolutionary behavior, however, is not set by the level of costs; rather it depends on the specific cost function that is assumed.

At convex cost functions for which $z = 0.7$, the resulting trade-off curves are concave; for linear cost functions in which $z = 1$, they consist of two linear parts and for concave cost functions in

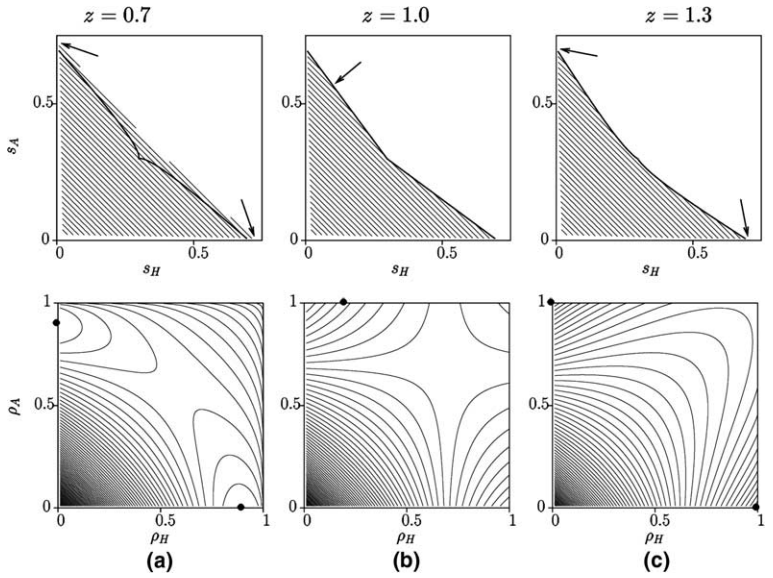

Fig. 4. Contour plots of total potential fitness s_{pot} (17) for the 'combined' cost functions. Costs parameters are all set to the intermediate level, and are all related to both the interference of intermediary products and to the trait values (11). Figures in the upper row show the fitness contours in terms of potential autotrophic and heterotrophic fitness, s_A and s_H. Here the feasibility sets $\mathscr{F}$ become visible; their boundaries form the trade-off curves $\mathscr{C}$. Solid lines other than the fitness contours show the boundaries of affinity trait space $\mathscr{B}$. Arrows indicate the evolutionary end strategies. Invasion boundaries are not shown but are all linear and intersect with the trade-off curve such that the singular strategies or boundary maxima are all attractors. Figures in the lower row show the fitness contours in terms of the affinities, ρ_A and ρ_H. Here, dots indicate the end points of evolution; these correspond to the arrows above. (a) The resulting trade-off is, although only slightly curved, convexly shaped. Evolutionary branching may occur and the population will then end up at pure strategies with sub-maximal affinity values. (b) The trade-off curve consists of two linear parts. The population will remain on the boundary maximum; (c) The trade-off curve is convex. The singular strategy is a branching point, at which the population may split up and evolve into pure autotrophs and pure heterotrophs with maximal affinity values.

which $z = 1.3$, they consist of two convex parts. For the fourth type of cost function, resulting trade-off curves consist of two linear parts again. None of these cost functions results in a convex trade-off curve; hence, none of these will lead to evolutionary branching.

The upper row of Fig. 4 shows the feasibility sets $\mathscr{F}$ and trade-off curves $\mathscr{C}$ resulting from the combined cost functions. In these cost functions the three relations between costs and trait values were combined with extra costs for interference; all costs were set to intermediate levels. Again, arrows show the strategies at which the population will end up. The lower row shows the corresponding contour plots in the affinity trait space. Here, dots indicate the end strategies.

It can be seen that for the first combined cost function (Fig. 4(a)) the trade-off curve is convex and does not coincide with the trait boundaries. Evolutionary branching may occur and simulations show that the population will then end up consisting of pure autotrophs ($\rho_A = 0.8$, $\rho_H = 0$) and pure heterotrophs ($\rho_A = 0$, $\rho_H = 0.8$); notice that eventually both types have a sub-maximal affinity for the function in which they specialize. A combined cost function with $z = 1$ leads to a trade-off function that consists of two linear parts, resulting in a singular strategy that also is a

boundary optimum (CSS) (Fig. 4(b)). The shape of this curve coincides largely with the boundaries of affinity trait shape; only its center does not. A combined cost function with $z = 1.3$ leads to a trade-off that is convexly shaped (Fig. 4(c)) and completely coincides with the boundaries of the affinity values. For this trade-off curve the population will evolve towards a branching point at which the population splits up. Eventually it will end up in pure autotrophs ($\rho_A = 1$, $\rho_H = 0$) and pure heterotrophs ($\rho_A = 0$, $\rho_H = 1$); both types will thus have a maximum affinity for the function in which they specialize.

4. Discussion

4.1. Intrinsic vs. extrinsic properties

Intrinsic properties affect the organism's *potential* fitness, while extrinsic properties affect the environment and therefore the *actual* fitness of the organism. Intrinsic properties considered in this study are the level of the costs, the mechanisms underlying these costs and the constraints on the affinity trait space. With extrinsic properties are meant external environmental properties such as the total carbon or nitrogen content and the incoming light intensity.

The intrinsic and extrinsic properties affect the system's evolutionary behavior each in a different way. Following Levins' extended approach, the evolutionary outcome of a system is determined by the shape of the trade-off curve and that of the invasion boundaries. As was discussed above, the trade-off curve is based on the boundaries of the feasibility set and is therefore only affected by intrinsic properties. In contrast, invasion boundaries do depend on the environment and theoretically they can thus be affected by extrinsic properties.

Remarkably, however, it was found that the environmental properties do not have any effect on the evolutionary outcomes at all, which was shown in Appendix A. This result is explained by the mass balance that was respected in the model: the feedback mechanisms that take care of the full material recycling in the system couple the steady state densities of the environment such that even under different environmental conditions the mixotrophs will evolve to the same strategy.

Although this result was derived for a closed system, it can be easily extended to open systems. Changing the closed system into an open system can be done by adding in- and output fluxes to the equations that describe the changes in the state variables (1a), (1b), (1c) and (1d). For the mixotroph system, an obvious choice would be to have DIC and DIN enter the system, and to have detritus removed as is often the case in the surface layer of a water column. Another possibility would be a constant flow of water in and out of the system, carrying a certain concentration of compounds, such as in a chemostat environment. By consequently adjusting the equations in the appendix as to include these in- and output fluxes, it can be shown that in such open systems the evolutionary behavior would be affected not only by intrinsic parameter values, but also by the parameters that determine these in- and output fluxes (e.g. the dilution rate). If these fluxes are very large, they will come to dominate the system's evolutionary behavior. For example, when the influx of DIC and DIN is very large as well as the outflux of detritus, the autotrophs will be no longer dependent on heterotrophs and are able to survive on their own. Surely, in such an environment it will be advantageous to specialize into more autotrophic organisms. On the other hand, as the in- and output fluxes go to zero, the evolutionary behavior of the system will

become dominated more and more by intrinsic parameters. Eventually, the system will be completely closed as the one studied in this paper, and its evolutionary behavior will be determined by intrinsic parameters only.

4.2. Boundaries of the affinities' trait space

Fig. 3 shows that many of the trade-off curves $\mathscr{C}$ coincide with the boundaries of affinity trait space $\mathscr{B}$. This happens if fitness increases monotonously in both affinities, instead of having an internal optimum. If coinciding with the trade-off curve, these boundaries determine to what value the fitness can increase. Singular strategies on such trade-off curves will thus always lie on (one of) the extremes of the affinity trait space, and will in that sense be boundary maxima. Usually, at a singular strategy both the fitness gradients vanish (14). At the singular strategies that lie at a boundary of the affinity trait space, only one of these gradients will be zero.

The influence of the trait space boundaries becomes apparent in the shape of the trade-off curve, which explains the pointed shapes that many of them have. Along the boundaries of the affinity trait space, one of the traits is held constant at a value of 1. At their 'tips', which in affinity trait space corresponds to the strategy of ($\rho_A = 1$, $\rho_H = 1$), the control of the trade-off curve switches from one boundary to another. At such a tip, neither of the fitness gradients is zero.

This illustrates that the constraints on the affinities can greatly control the location of the singular strategy and the shape of the trade-off curve. In this way they can have considerable effect on the evolutionary outcomes of the system.

4.3. Cost level

The level of the costs also has considerable effects on the evolutionary behavior of the system. If costs are small relative to the benefits, the trade-off between autotrophic assimilation and heterotrophic assimilation will be very weak, which results in a feasibility set that is 'pointing outward', as can be seen in the first column of Fig. 3. Small costs hardly put any constraints on the affinity values, even when the cost function is convex. In this case it is advantageous to increase the affinities to their maximum, which explains why for low cost levels the evolutionary behavior is governed completely by the boundaries of the trait space. The corresponding evolutionary outcome will be a population ending up at the boundary optimum lying at the 'tip' of the trade-off curve which, as mentioned above, corresponds to a strategy of ($\rho_A = 1$, $\rho_H = 1$). At this strategy the population will remain (CSS).

At intermediate costs, the trade-off is stronger which is visible from the feasibility set that has become smaller and has flattened. In some cases (Fig. 3(e) and (h)) the trade-off curve is still determined by the constraints on affinities; this is, however, largely related to the cost function at hand. In other cases (Fig. 3(b) and (k)), the trade-off curve is (at least partially) governed by the relation of affinities with costs and benefits. The singular strategy has shifted over the trade-off curve in the upper left direction, which in terms of trait values means that the affinity for the heterotrophic route has decreased.

If costs are high, the population will evolve to 'the extreme' of the trade-off curve, where the affinity for the heterotrophic route has decreased to zero ($\rho_H = 0$) and organisms are pure autotrophs. Monomorphic populations consisting of a strategy in which one of the trait values is zero

are not viable, as they can not maintain a complete nutrient cycle; as a consequence, such populations will die out. The phenomenon in which the population evolves towards a non-viable strategy is called evolutionary suicide [18,19]. As low costs lead to a boundary optimum that is a CSS while high costs lead to evolutionary suicide, a branching point can only be found at intermediate cost levels.

4.4. Cost function

The cost function specifies the relation between costs and affinity. To a large extend, this relation determines whether a trade-off curve is controlled by the boundaries of affinity trait space or not. Costs that increase with affinity in a convex manner ($z > 1$) turn out relatively high for small affinities but level off for higher affinities. Therefore, high affinities will be relatively cheap and these strategies will naturally lead to the highest potential fitnesses. As in such case the potential fitness will be increasing monotonously in the two affinities, it are the boundaries set to the affinity trait space that determine the curvature of the trade-off curve (Fig. 3, third row). In contrast, concave cost functions ($z < 1$) lead to relatively low costs at small affinities. This leads to a fitness optimum at intermediate affinities, in which case the boundaries of the trait space do not affect the trade-off curve (Fig. 3, first row). Also for linear cost functions ($z = 1$), high affinities are relatively cheap. This is a consequence of the division of the assimilation flux $j_{V,A}$ by the yield coefficient $y_{C,V}$ (5): whereas both the assimilation flux and the costs depend linearly on the affinities, only the assimilation flux goes through the origin; the cost function is set off by the base cost y^0, which is always larger than zero (11). Therefore, also for linear cost functions the trade-off function is controlled by the boundaries of affinity trait space (Fig. 3, second row).

The effect that the cost function has on the evolutionary behavior can be read from the shape of the trade-off curve. For costs that increase with trait values in a convex manner ($z < 1$) the trade-off curve is concavely shaped (Fig. 3, first row). In combination with invasion boundaries that are linear and singular strategies that are attracting, concave shaped trade-off curves will always lead to continuously stable strategies (CSS's).

For costs that are linearly related to trait value ($z = 1$), trade-off curves consist of two straight lines connected at a blunt angle (Fig. 3, second row). Linear costs put an advantage to higher affinities; at the boundaries, where one of the affinities is constant, these costs increase linearly with the other affinity. This explains why the two parts of the trade-off curve are linear as well (Fig. 3(d)–(f)). At intermediate costs the singular strategy will lie somewhere on the upper segment of the trade-off curve. Once such a strategy is reached, the invasion boundary coincides with this straight part of the trade-off curve which means that all strategies on this part of the trade-off curve will then have the same invasion fitness. In practice, the population will remain on such a strategy.

Concavely shaped cost functions ($z > 1$) will give rise to trade-off curves that consist of two segments that are both convexly curved (Fig. 3, third row). This is because at the boundaries, where one of the affinities is held constant, costs still increase convexly and specialized strategies are favored over mixed ones. Like before, at intermediate cost levels the singular strategy will have shifted to the middle of the upper segment of the trade-off curve. Once the population has reached this strategy, this segment will lie above the invasion boundary, and all strategies on this part of the trade-off function are able to invade. This combination of trade-off curve and invasion bound-

ary indicates that the system has a branching point at which the population will split into two populations. However, the two resulting populations will consist not of pure autotrophs and pure heterotrophs, but of pure autotrophs ($\rho_A = 1$, $\rho_H = 0$) on the one hand and mixotrophs ($\rho_A = 1$, $\rho_H = 1$) on the other. So basically, only one of the traits is involved in the process of evolutionary branching, while the other trait remains constant.

Trade-off curves resulting from the fourth cost function ($y^{AH} > 0$), in which costs are related to the interference of intermediate products, consist of two straight parts again (Fig. 3, fourth row); this is because the trade-off curve is determined by the limited boundaries of trait space, and at these boundaries the costs will increase linearly. This cost function only affects mixed strategies; strategies towards the zero-boundaries are much less affected and completely pure strategies are not affected at all, which explains why the extremes of the trade-off curve are equal at all three levels of costs. At intermediate costs, the singular strategy will lie somewhere at the upper segment of the trade-off curve and the population will remain on this singular strategy.

4.5. Evolutionary branching

None of the simple cost functions discussed above leads to a convex trade-off curve; and thus, none of them leads to a branching point. Fig. 4, however, shows that some of their combinations do lead to convex trade-off curves. In these 'combined' cost functions, two mechanisms are assumed to underlie the costs simultaneously: one part of the costs is related to the value of the affinities, and another part is related to the interference between the two affinities. As discussed earlier, the relation between affinities and costs determines whether the fitness optimum lies at intermediate affinities or at maximum affinities values. The costs for interference put a disadvantage to maximizing both traits at the same time, which favors pure strategies over mixed ones. Apparently, it is the combination of these costs that make a convex trade-off curve possible and thus evolutionary branching. To understand this finding, we will discuss the different combinations one by one.

In the first case (Fig. 4(a)), the costs of interference are combined with a concave cost function ($z = 0.7$). Owing to the contribution of the concave cost function, the potential fitness optima come to lie at intermediate affinity values, and the boundaries of the trait space do not play a role in shaping the trade-off curve. Simultaneously, the costs for interference favor pure strategies over mixed ones, which in this case is enough to provide an advantage to specialization. Indeed this cost function leads to a trade-off curve that, although only slightly curved, is clearly convexly shaped and may lead to evolutionary branching of the population.

In the other cases (Fig. 4(b) and (c)), the boundaries of the trait space do affect the trade-off curve, and the formation of its curvature is more complicated. When the trait space boundaries control the trade-off curve, the behavior of the cost function at these boundaries is important. At the boundaries one of the affinities is constant; for the costs related to interference, which are proportional to the product of the affinities, this means that they will increase linearly with the other affinity. Hence, in contrast to the previous case, these costs will now not induce an advantage to specialization. Costs that are related linearly to affinity ($z = 1$) will not favor specialization either. As a result, the trade-off curve will consists of two linear parts (Fig. 4(b)). Consequently, the boundary optimum will not be a branching point, and the population will remain on this strategy. In contrast, if the costs related to affinity are concave ($z > 1$), these will favor specialized strategies over mixed ones, even at the boundaries of trait space. Standing alone, these

costs led to a trade-off curve that resulted in branching in only one of the traits (see Fig. 3(h)); however, in combination with costs for interference that discourages mixed strategies, the two convex parts are connected such that a completely convex trade-off curve results (Fig. 4(c)). This gives rise to a branching point and specialization may now occur.

In summary, a single mechanism underlying the costs will not result in evolutionary branching; it is the combination of two mechanisms with complementary effects that can lead to a convex trade-off curve and thus to a branching point. In both cases that a branching point does arise, the mechanisms together combine into an explicit advantage to specialization. Apparently, such an advantage must exist explicitly in the underlying metabolic mechanisms in order to obtain evolutionary branching. Usually, mechanisms such as interference between the two affinities could already introduce such an advantage and hence evolutionary branching. For the studied system, however, this is not the case due to the constraints imposed on the affinities. As a result of these constraints, only some of the more complicated cost functions may now induce evolutionary branching. This clearly illustrates the considerable consequences that constraints on the trait space can have for the evolutionary outcomes of the system.

5. Conclusions

We have studied a DEB model of a population of mixotrophs and the conditions under which this population will specialize into separate autotrophs and heterotrophs. For the mixotrophic organisms a trade-off exists between autotrophy and heterotrophy, which was derived from the physiological mechanisms in the DEB model. Difficulties in applying the AD theory, which were inherent to the model's complexity and its two-dimensionality of the trait space, could be solved by using the extended version of Levins' graphical approach. This approach was particularly helpful in providing more insight in the effects of the various mechanisms on the curvature of the trade-off function, and therefore on the system's evolutionary outcome.

The evolutionary behavior of the mixotrophic population was found to depend only on intrinsic properties such as the cost function (the relation between the costs and the affinities for assimilation) and the level of these costs; also the boundaries of the affinity trait space were found to play an important role. Evolutionary branching was found to occur only at intermediate cost levels and for cost functions that create an explicit advantage to specialization. Although this might seem obvious, it may not always be realized when assuming a specific trade-off function without considering the underlying mechanisms.

Furthermore, it was found that the constraints on the affinities can greatly affect the location of the singular strategy and the shape of the trade-off curve. As such they can considerably complicate the requirements for evolutionary branching. This result should be taken into account when considering trade-offs from real systems, because in the natural situation many constraints might exist on physiological processes and the associated parameter values.

In contrast to the intrinsic properties, extrinsic properties such as total nutrient content were found to have no effect on the evolutionary outcomes of the model at all. This was related to the mass balance and the feedback mechanisms in the system. Hence, our analysis suggests that evolutionary branching of the mixotrophic population is not a common feature of the system and

that it is not related to the environment. This, perhaps, explains the observations in the introduction that many organisms are in fact mixotrophic, and that mixotrophs are found in a range of eutrophic to oligotrophic waters. However, assumptions such as homogeneity and the application of the mass balance may limit the possibilities for evolutionary branching and specialization. Additional research could therefore study the effects that for instance spatial structure has on the evolutionary behavior of the system.

Another line of research could make use of the fact that the mixotroph model presented in this study consists of only a single population, which makes it one of the smallest non-degenerative ecosystems that we can think of. Evolutionary branching into separate autotrophic and heterotrophic populations forms the first step in the evolution of the ecosystem to develop from a very simple to a more complex (and realistic) ecosystem, purely by self organization. It would be interesting to study this process of self-organization, and to follow the developments that take place in the cycling of energy and nutrients.

Acknowledgments

We would like to thank Hans Metz, Claus Rueffler and Michel Durinx for their help and suggestions on this work.

Appendix A. Extrinsic properties have no effect on the evolutionary outcomes

In a homogeneous system, the singular strategy and its evolutionary stability are determined only by parameters that are intrinsic to the organisms. This means that they are not affected by environmental properties such as the total nitrogen content, the total carbon content or the incoming light intensity. This can be shown as follows:

As a time scale separation is assumed between the evolutionary and ecological dynamics, the resident population is considered to be always in steady state with its environment. The resident's fitness s_{res} is equal to its specific growth rate (15), which in steady state must be equal to zero(12):

$$s_{\text{res}} = \frac{j_{\text{V,A}}(\rho_{A_{\text{res}}}, \rho_{H_{\text{res}}}, E_{\text{res}})}{y_{\text{C,V}}(\rho_{A_{\text{res}}}, \rho_{H_{\text{res}}})} - k_{\text{M}} - h = 0 \tag{18}$$

This can be rewritten into the following expression for the total assimilation flux. (The star denotes that a flux is constant on a ecological time scale, but may vary on an evolutionary time scale.)

$$j^*_{\text{V,A}} = (k_{\text{M}} + h) y_{\text{C,V}}(\rho_{A_{\text{res}}}, \rho_{H_{\text{res}}}) \tag{19}$$

Since the system is assumed to be in steady state, the density of detritus is constant; $\frac{\text{d}}{\text{d}t} X_{\text{D}} = 0$. The detritus density depends on the specific detritus uptake flux (for autotrophic assimilation) $j_{\text{D,A}_H}$ and the specific influx of detritus, which is equal to the specific death rate h (1c). Therefore, in steady state $j^*_{\text{D,A}_H} = -h$. The uptake flux of detritus is determined by the heterotrophic

assimilation flux j_{V,A_H} and the yield coefficient of biomass from detritus $y_{D,V}$ (4). With the steady state assumption, (1c) and (4) can be combined into an expression for the heterotrophic assimilation flux:

$$j^*_{V,A_H} = \frac{h}{y_{D,V}} \tag{20}$$

By substituting (19) and (20) in (8), an expression for the autotrophic assimilation flux can now be given as well:

$$j^*_{V,A_A} = (h + k_M) y_{C,V}(\rho_{A_{res}}, \rho_{H_{res}}) - \frac{h}{y_{D,V}} \tag{21}$$

Substituting (20) and (21) in respectively (6) and (7) yields expressions for the steady state functional responses f^*_A and f^*_H:

$$\begin{aligned} f^*_A &= \frac{(h + k_M) y_{C,V}(\rho_{A_{res}}, \rho_{H_{res}}) - \frac{h}{y_{D,V}}}{\rho_{A_{res}} j_{V,A_A m}} \\ f^*_H &= \frac{\frac{h}{y_{D,V}}}{\rho_{H_{res}} j_{V,A_H m}} \end{aligned} \tag{22}$$

The steady state values of both these functional responses can thus be fully expressed in terms of $\rho_{A_{res}}$ and $\rho_{H_{res}}$ and other intrinsic parameters that are constant both on an ecological and an evolutionary time scale (h, k_M, $y_{D,V}$, z, $j_{V,A_A m}$, $j_{V,A_H m}$, y^0, y^A, y^H and y^{AH}).

In turn, the functional responses determine the steady state densities of DIC (X_C), DIN (X_N) and detritus (X_D). This is done via Eqs. (9) and (10), such that for a given set of system properties (X_{C+}, X_{N+}, and $j_{L,F}$) the invasion fitness of the residents is exactly zero:

$$E_{res} = \{X_C, X_N, X_D | X_{C+}, X_{N+}, j_{L,F}, s_{res} = 0\} \tag{23}$$

As follows from (13) and (15), the invasion fitness of a mutant invading in a resident population depends on its phenotype ($\rho_{A_{mut}}, \rho_{H_{mut}}$) but also on the environment as was set by the residents E_{res} and thus on the environmental properties. However, from (9) and (10) it can be seen that the mutants have exactly the same steady state functional responses as the residents; (22) showed that these functional responses do not depend on environmental properties but only on intrinsic parameters:

$$f_{A_{mut}} = f^*_A \quad \text{and} \quad f_{H_{mut}} = f^*_H \tag{24}$$

By substituting (24) in (16), the environmental properties can be 'bypassed' in calculating the invasion fitness of the mutants. That is, we do not need the steady state values of DIC, DIN and detritus to calculate the steady state functional responses and the associated invasion fitnesses of the mutants. Eq. (13) can thus be replaced by

$$s_{mut} = r(\rho_{A_{mut}}, \rho_{H_{mut}}, \rho_{A_{res}}, \rho_{H_{res}}) \tag{25}$$

The invasion fitness of a mutant invading a resident population can thus be fully expressed by intrinsic parameters. From the invasion fitness, the invasion boundaries and the shape of the

trade-off curve can be determined; or, for a more analytical approach, the fitness gradients (14), the location of the singular strategies and their evolutionary stability can be calculated. Therefore, the evolutionary outcomes of the system can also be determined from intrinsic parameters alone. In other words, these evolutionary outcomes are not affected by the environmental properties at all.

This result can be explained by the feedback mechanisms in the system, which couple the densities of detritus (needed for heterotrophy) with the densities of DIC and DIN (needed for autotrophy). As a consequence, these densities can not vary independently; changing one of the system properties will directly or indirectly affect all densities. Because the system is closed, for any set of environmental properties a balance is sought between autotrophy and heterotrophy, which apparently always results in the same evolutionary outcome.

References

[1] H.L. Stickney, R.R. Hood, D.K. Stoecker, The impact of mixotrophy on planktonic marine ecosystems, Ecol. Modell. 125 (2000) 203.
[2] D.K. Stoecker, Conceptual models of mixotrophy in planktonic protists and some ecological and evolutionary implications, Eur. J. Protistol. 34 (1998) 281.
[3] K.R. Bockstahler, D.W. Coats, Spatial and temporal aspects of mixotrophy in chesapeake bay dinoflagellates, J. Euk. Microbiol. 40 (1993) 49.
[4] D.A. Holen, The relative abundance of mixotrophic and heterotrophic ciliates in an oligotrophic lake, Arch. Hydrobiol. 150 (2000) 1.
[5] J.A. Raven, Phagotrophy in phototrophs, Limnol. Oceanogr. 42 (1997) 198.
[6] T.F. Thingstad, H. Havskum, K. Garde, B. Riemann, On the strategy of "eating your competitor": a mathematical analysis of algal mixotrophy, Ecology 77 (1996) 2108.
[7] G. Wachtershauser, Pyrite formation, the first energy source for life: a hypothesis, Syst. Appl. Microbiol. 10 (1988) 207.
[8] S.A.L.M. Kooijman, R. Hengeveld, The symbiontic nature of metabolic evolution, in: T.A.C. Reydon, L. Hemerik (Eds.), Current Themes in Theoretical Biology: A Dutch Perspective, Springer, 2004, pp. 159–202.
[9] H. Hartman, Photosynthesis and the origin of life, Origins Life Evol. Biosphere 28 (1998) 515.
[10] S.A.L.M. Kooijman, Dynamic Energy and Mass Budgets in Biological Systems, 2nd Ed., Cambridge University, 2000.
[11] J.A.J. Metz, S.A.H. Geritz, G. Meszéna, F.J.A. Jacobs, J.S. Heerwaarden, Adaptive dynamics a geometrical study of the consequences of nearly faithful reproduction, in: S.J. van Strien, S.M. Verduyn Lunel (Eds.), Stochastic and Spatial Structures of Dynamical Systems, Elsevier, 1996, p. 183.
[12] S.A.H. Geritz, E. Kisdi, G. Meszéna, J.A.J. Metz, Evolutionary singular strategies and the adaptive growth and branching of the evolutionary tree, Evol. Ecol. (1998) 35.
[13] C. Rueffler, T. van Dooren, J.A.J. Metz, Adaptive walks on changing landscapes: Levins' approach extended, Theor. Pop. Biol. 65 (2004) 165.
[14] S.A.L.M. Kooijman, H.A. Dijkstra, B.W. Kooi, Light-induced mass turnover in a mono-species community of mixotrophs, J. Theor. Biol. 214 (2002) 233.
[15] S.A.L.M. Kooijman, The synthesizing unit as model for the stoichiometric fusion and branching of metabolic fluxes, Biophys. Chem. 73 (1998) 179.
[16] G. Meszéna, E. Kisdi, U. Dieckmann, S.A.H. Geritz, J.A.J. Metz, Evolutionary optimisation models and matrix games in the unified perspective of adaptive dynamics, Selection 2 (2001) 193.
[17] R. Levins, Theory of fitness in a heterogeneous environment. i. The fitness set and adaptive function, Am. Natural. 96 (1962) 361.

[18] M. Gyllenberg, K. Parvinen, Evolutionary suicide and evolution of dispersal in structured metapopulations, J. Math. Biol. 45 (2002) 79.
[19] M. Gyllenberg, K. Parvinen, Necessary and sufficient conditions for evolutionary suicide, Bull. Math. Biol. 63 (2001) 981.